JOURNAL OF MATERIALS SCIENCE 19 (1984) 3121–3139

Review
The role of alloying elements in the design of nickel-base superalloys

A. K. JENA
Department of Metallurgical Engineering, Indian Institute of Technology, Kanpur, India
M. C. CHATURVEDI
Department of Mechanical Engineering, University of Manitoba, Winnipeg, Manitoba, Canada

The constituents of nickel-base superalloys have been classified into solid solution formers, precipitate formers, carbide formers and surface stabilizers. The characteristics of solutes which would make them most suitable in each category have been specified and appropriate alloying elements have been identified. Nickel-base superalloys are hardened primarily by the precipitation of Ni_3X type compounds. The occurrence and crystallography of precipitation of various kinds of Ni_3X type precipitates have been considered. The role of substitution by alloying elements on mismatch and stability of phases has been discussed. The free electron model and the Engel–Brewer model have been applied for evaluating the stabilities of precipitates, and the role of the alloying elements in determining the stabilities of external and internal surfaces such as grain boundaries have been briefly outlined.

1. Introduction

Superalloys are now widely used in a variety of applications at temperatures ranging from 923 to 1373 K in aggressive atmospheres such as the combustion products of fuel and air, high temperature cataytic reactors etc. [1]. In order to function satisfactorily in such a severe environment superalloys must possess properties such as outstanding high temperature strength, creep and fatigue resistance, excellent ductility, good impact resistance and adequate resistance to hot-corrosion [2]. The unique set of properties required in these alloys is obtained by having an f c c matrix which is hardened by solutes and precipitates. The precipitates in nickel-based superalloys are primarily Ni_3(AlTiNb) type intermetallic compounds and carbides and are of suitable structure, shape, size and distribution so as to give the desired properties and to resist microstructural changes at high temperatures. The functions of alloying constituents in superalloys must be clearly understood to make a judicious choice of alloying additions and thus optimize the properties.

A number of reviews have been published on the defect structure and precipitate-defect interactions [3], microstructural characteristics [4] and structure property relations [5] in nickel-base superalloys. The roles of impurities and trace elements have been reviewed by Holt and Wallace [6]. Since the publication of these reviews a great deal of work has been done and considerable progress has been made in the understanding of the role of various constituents of nickel-base superalloys. In the review presented here, the constituents have been classified into solid solution formers, precipitate formers, carbide formers and surface stabilizers. The role of each constituent element has been critically assessed. The precipitate formers have been discussed in greater detail. The occurrence of Ni_3X type compounds, their structure, crystallography of their precipitation, role of alloying additions on the coherency

0022–2461/84 $03.00 + .12

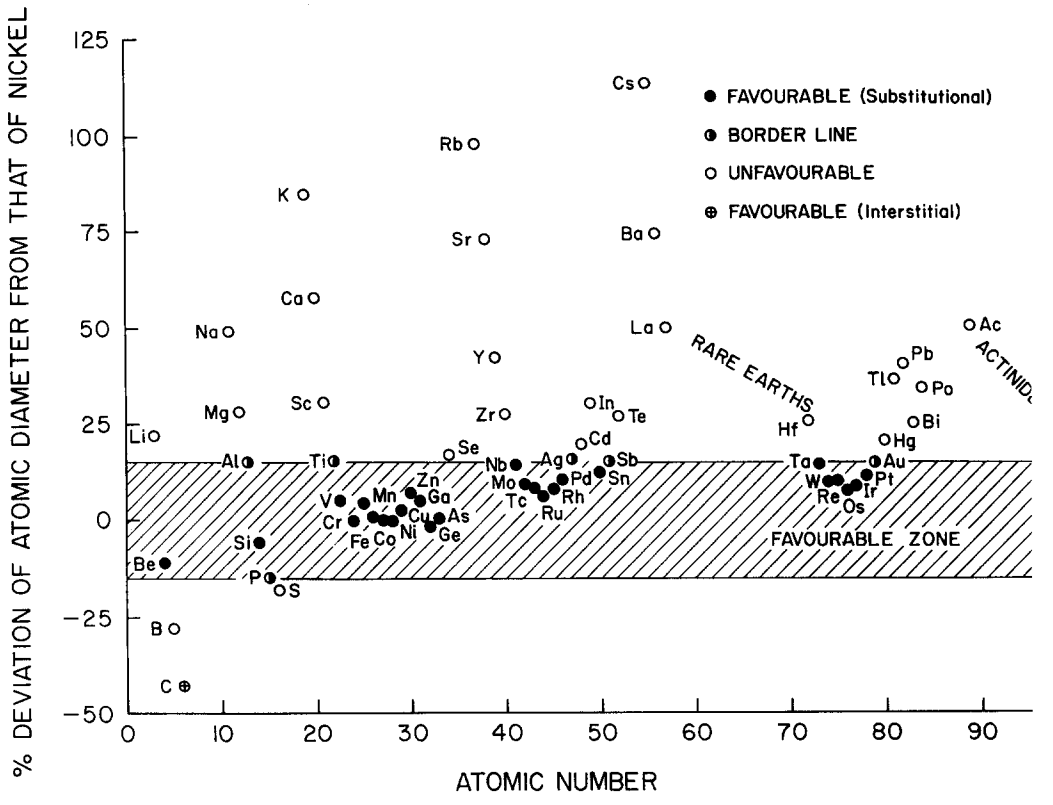

Figure 1 Atomic size factors of elements for solid solution formation with nickel.

of these precipitates have been considered. The free electron concentration approach as well as the Engel–Brewer approach for predicting the stabilities of precipitates and the effects of substitution of alloying elements on their stabilities have been critically examined.

2. Solid solution formers

The primary function of solid solution formers is to impart strength to the matrix. Solutes having reasonable solid solubility and high hardening coefficients can result in appreciable solid solution hardening and should also improve the creep strength of the matrix.

The solubility of various elements in nickel can be assessed by plotting a size factor function $[d_{Ni}[100(d_i - d_{Ni})/d_{Ni}]$ of an element i, with a diameter d_i, against its atomic number. In the size factor function expression d_{Ni} is the atomic diameter of nickel. Fig. 1 shows such a plot for various elements. The shaded zone in this figure contains values of the function between + 15 and − 15. If the size factor function of an element falls within this zone, appreciable solid solubility of an element in nickel is expected [8]. An examination of available data on the solid solubility of elements in nickel [9] shows that all the elements having size factor functions (Fig. 1) on the borderline are soluble in nickel except silver and phosphorus. Thus, the elements beryllium and titanium from Groups IIA and IVA, all the elements of Groups VA to VIIIA and the elements copper, gold, zinc, aluminium, gallium, silicon, germanium, tin, arsenic and antimony from Groups IB to VB may have significant solubility in nickel. Indium appears to be the only exception. Its solubility in nickel is about 15% although the size factor function is not favourable (Fig. 1). If, however, complete ionization of indium [8] is assumed, the size factor function is near the borderline.

The solid solution forming elements increase the strength of the solution by primarily increasing the resistance to the movement of dislocations. This resistance arises from distortions and shear modulus changes in the lattice due to solute atoms and more difficult cross slipping of dissociated dislocations in solid solutions where the stacking fault energy has been lowered as a result of alloying. The average lattice distortion due to atomic size difference between nickel and the solute is

TABLE I Solid solution hardening parameters of elements having significant solubility in nickel

Element i	Melting temperature (K)	% Change in the lattice parameter of nickel per atom % solute	$\frac{(d_i - d_{Ni})100^*}{d_{Ni}}$	Separation between the groups for nickel and the solute in the periodic table	Change of flow stress ($\epsilon = 0.0002$) per atom % solute, (MPa at $\%^{-1}$)
W	3650	0.135	10.0	4	16.5
Re	3453		10.0	3	
Os	3300	0.027	7.5	2	
Ta	3269		14.5	5	
Mo	2890	0.116	9.5	4	14.2
Nb	2740	0.169	14.5	5	
Ir	2727		9.0	1	
Ru	2700		6.5	2	
Tc	2490		8.5	3	
Rh	2239		8.0	1	
V	2190	0.049	5.2	5	
Cr	2176	0.032	0.2	4	4.9
Pt	2043	0.157	11.5	0	
Ti	1940	0.095	16.0	6	22.7
Pd	1823	0.136	10.5	0	
Fe	1809	0.031	1.3	2	3.3
Co	1768	0.005	0.2	1	0.3
Ni	1725				
Si	1693	−0.025	−5.5	4	
Be	1556		−10.5		
Mn	1517	0.082	4.5	3	
Cu	1357	0.025	2.5	1	1.6
Au	1336	0.216	15.5	1	
Ge	1232		−1.5	4	
As	1084		0.5	5	
Al	932	0.048	15.0	3	
Sb	904	0.153	16.5	5	
Zn	693		7.0	2	
Sn	505	0.246	12.5	4	
In	429		18.5	3	
Ga	303	0.055	5.3	3	

*d = atomic diameter.

given by the change in lattice parameter of the nickel-rich matrix caused by alloying. Pelloux and Grant [10] have shown that for the same magnitude of change in lattice parameter the increase in flow stress of nickel is greater when the separation between the groups for nickel and the solute in the Periodic Table is greater. Greater separation between the groups implies an increase of the electron hole number due to solutes like cobalt, iron, manganese, chromium, vanadium and titanium and an increase in electron to atom ratio in case of solutes like copper, zinc, and aluminium. The decrease in the stacking fault energy of nickel due to a solute is also generally greater when the separation between the nickel group and that of the solute in the Periodic Table is greater [11, 12]. Thus, solutes with large atomic diameters and from groups in the Periodic Table well separated from nickel are likely to harden the matrix. Table I lists these two factors for all the elements likely to be soluble in nickel. Data available [13, 14] on the percentage change of the lattice parameter of nickel due to 1 at% solute are also listed in Table I. They correlate well with the size factor function. For some elements the hardening coefficients defined as the increase in flow stress per unit percentage increase in solute content, are available [10]. These data are incorporated in the table. They also correlate well with the size factor function and the separation between groups of nickel and the solute.

The three important parameters which improve creep resistance of metals are low diffusivity, low stacking fault energy and high elastic modulus [10]. Fig. 2 is a plot of diffusion coefficients of a

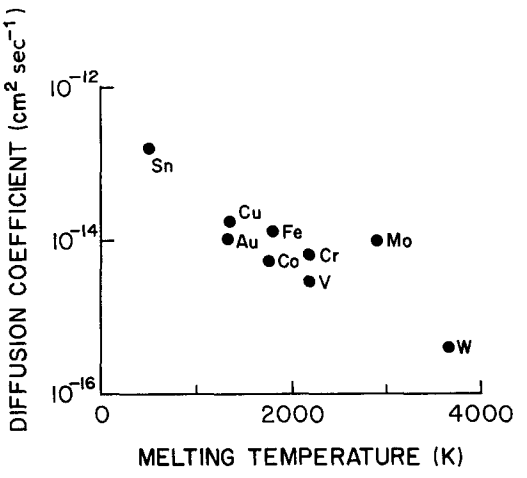

Figure 2 Change of diffusion coefficients of solutes in nickel at 1000 K with melting temperatures of solutes.

number of solutes in nickel [15] at 1000 K against their melting temperatures. It shows that higher the temperature of melting of the solute, the lower is its diffusivity. The high melting solutes are to be preferred for better creep resistance. Table I lists the solutes in order of decreasing melting temperatures. As pointed out above, decrease in stacking fault energy is related to the position of the solute in the Periodic Table. The solutes, however, may either increase or decrease the elastic modulus [16]. The elements tungsten, molybdenum and titanium have high melting points and high hardening coefficients. They are, therefore, most suitable solid solution formers, although their solubility in nickel is not very high. Other elements such as tantalum, niobium, vanadium, rhenium and technetium are high melting, have large atomic diameters and are from groups well separated from that of nickel. They should also be good solid solution formers. However, solid solution hardening coefficients of these elements are not available. The hardening coefficient of an element like chromium is small. But because of the high solubility of chromium (size factor function 0.2) in nickel and high chromium contents of superalloys, the contribution of chromium to solid solution hardening is appreciable. It has been estimated [5] that in an alloy containing 20% Co, 10% Fe, 20% Cr, 4% Mo, 4% W, 1.5% V, 6% Al, and 1% Ti, the contribution of chromium to solid solution hardening is 19%. The contributions to the solid solution hardening by aluminium and titanium are lost when these elements are removed from the matrix by precipitation. Change in composition of the matrix due to precipitation can be appreciable [17].

All elements soluble in nickel do not distribute themselves uniformly in the matrix; some tend to segregate to the grain boundaries. Segregation of copper, manganese, silicon and antimony to grain boundaries in nickel-base alloys has been detected by Auger electron spectroscopy and X-ray imaging techniques [18–20]. Segregation of copper may be eliminated by a long diffusion anneal, but segregation of manganese does not change appreciably [18]. Segregation of copper, manganese, silicon and antimony results in a reduction of hot malleability and creep ductility [18–20] due to grain-boundary cracking. An increase in inclusion content with increase in silicon also reduces hot ductility [18]. However, segregation of silicon and manganese to grain boundaries improves weldability [6]. Arsenic also reduces hot malleability [6, 21]. This characteristic is attributed to the segregation of arsenic to grain boundaries. Loss of creep ductility due to small percentages of tin in superalloys is attributed to the segregation of tin to the grain boundaries [20, 21]. However, a threefold increase in the stress rupture life of MAR-M200 at 1133 K has also been attributed to tin [6]. The role of tin needs to be more thoroughly investigated.

3. Precipitate formers

Solid solution strengthened alloys may be further strengthened by precipitation hardening. The precipitations increase the resistance to dislocation motion. Dislocations may either bow around the precipitates or cut through them [22]. The stress necessary for the dislocations to bow around precipitates is inversely proportional to the interparticle distance which increases with increase in particle size in a system which has a fixed volume fraction of precipitating phase. The stress required to cut the precipitate is proportional to the square root of its size. Hence the optimum strength is obtained when the interparticle spacing is just small enough to prevent the dislocations from bowing. The characteristics which determine the magnitude of stress required to cut the precipitates are: elastic coherency strains around the precipitate; antiphase boundary energy of ordered precipitates; precipitate–matrix interfacial energy; and the differences between the elastic moduli and stacking fault energy of precipitate and matrix.

A number of binary metallic compounds con-

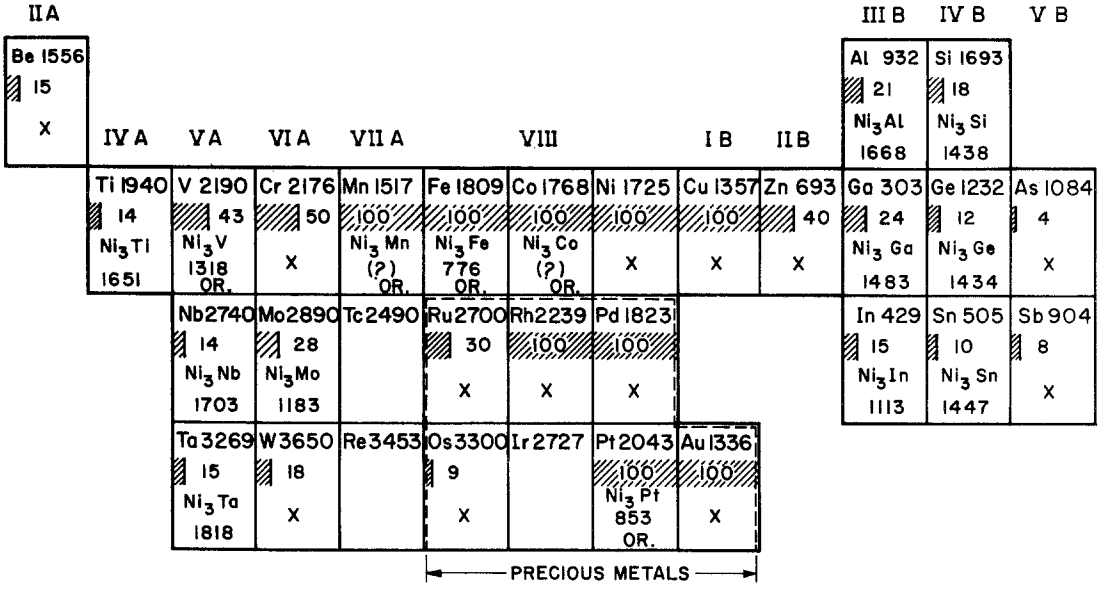

Figure 3 Occurrence of Ni_3X type compounds (see text for explanation).

taining about 75 at% Ni have an ordered cubic $L1_2$ structure. These ordered compounds are likely to precipitate coherently and strengthen the nickel-rich matrix.

3.1. Occurrence of Ni_3X type compounds

Fig. 3 shows the occurrence of Ni_3X type compounds [9] in various Ni–X systems where X represents elements with some solid solubility in nickel (Fig. 1). The elements are arranged in Fig. 3 according to their position in the Periodic Table. Each rectangular space allotted to an element in this figure contains the symbol of the element and its melting temperature (in K) at the top. The shaded area and the associated number represent the maximum solubility of the element in nickel in at%. The compound Ni_3X, if present, is given next along with the upper temperature of its stability. The letters OR at the bottom of the rectangular space indicate that the compound is formed by an ordering reaction from the solid solution. A cross indicates absence of Ni_3X phase.

A number of elements form Ni_3X type compounds. The compounds in the systems containing manganese, iron, cobalt and platinum are formed at low temperatures as a result of an ordering reaction. High temperature strengthening due to precipitation in these systems is therefore unlikely. The rest of the elements aluminium, titanium, vanadium, niobium, tantalum, molybdenum, gallium, indium, silicon, germanium and tin form Ni_3X type compounds which are stable up to relatively high temperatures. Amongst all these compounds only Ni_3V forms by ordering and the rest are formed by peritectic or peritectoid reactions. The solubilities of these compounds in nickel decrease rapidly with decrease in temperature. These alloys are, therefore, likely to be suitable for precipitation. All these systems except the Ni–Mo system do not contain any compound containing greater than 75 at% Ni. Ni_4Mo is a stable compound, but the recently reported compound, Ni_8Ta, is of uncertain stability [23]. These compounds are unlikely to interfere with the precipitation reaction.

3.2. Crystal structures of Ni_3X type compounds

The crystal structures and lattice parameters of the Ni_3X type compounds [13] are listed in Table II. The compounds Ni_3Al, Ni_3Ga, and Ni_3Ge are ordered cubic. Ni_3Ti has an ordered hexagonal structure. Ni_3In and Ni_3Sn are also ordered hexagonal but their c-axis is nearly half of that of Ni_3Ti. Ni_3V and the high temperature modification of Ni_3Ta are ordered tetragonal. The structures of Ni_3Nb, the low temperature modification of Ni_3Ta and Ni_3Mo are ordered orthorhombic. Although the structures of these compounds appear to be widely different from each other and from the f c c structure of nickel, the atomic arrangements in all these structures are quite similar.

TABLE II Structural characteristics of Ni_3X type compounds

Element X in Ni_3X	Designation of the compound	Upper temperature of stability of the compound (K)	Structure	Lattice parameters ($\times 10^{-10}$ m)	Misfit, $\frac{(D_{ppt} - D_{Ni})100}{D_{Ni}}$
Al	γ'	1668	$L1_2$ Cu_3Au type	$a = 3.567$	1.2
Ti	η	1651	$D0_{24}$ Ni_3Ti type	$a = 5.1010$ $c = 8.3067$	2.4
V	γ''	1318	$D0_{22}$ Al_3Ti type	$a = 3.5424$ $c = 7.1731$	0.5, 1.2
Nb	β	1703	— Cu_3Ti type	$a = 5.11$ $b = 4.25$ $c = 4.54$	2.5, 4.6
Ta	β	1593	— Cu_3Ti type	$a = 5.115$ $b = 4.25$ $c = 4.542$	2.6, 4.9
	γ''	1818	$D0_{22}$ Al_3Ti type	$a = 3.627$ $c = 7.455$	2.9, 4.4
Mo	β	1183	— Cu_3Ti type	$a = 5.064$ $b = 4.223$ $c = 4.449$	1.6, 2.7
Ga	γ'	1483	$L1_2$ Cu_3Au type	$a = 3.5823$	1.7
In	Ni_3In	1113	$D0_{19}$ Ni_3Sn type	$a = 5.331$ $c = 4.251$	7.0
Si	γ'	1313	$L1_2$ Cu_3Au type	$a = 3.504$	−0.6
	—	1398	—		—
	—	1438	—		—
Ge	γ'	1434	$L1_2$ Cu_3Au type	$a = 3.566$	1.2
Sn	Ni_3Sn	1250	$D0_{19}$ Ni_3Sn type	$a = 5.293$ $c = 4.244$	6.2
	—	1447	—	—	—

The arrangement of atoms in f c c nickel (Al) is identical with that in the $L1_2$ structure, if orderin in the latter is ignored (Fig. 4). The close packed (1 1 1) planes are stacked in both in the same sequence, ABC. Fig. 5a shows the atomic arrangement in the (1 1 1) plane of the $L1_2$ structure. Alternate positions in alternate rows parallel to the [1 1 0] directions are occupied by the solute atoms which form a triangular network. This kind of ordering is called triangular. The ordered (1 1 1) planes are stacked so as to avoid solute–solute contacts. The ABC stacking sequence in the $L1_2$ structure is shown in Fig. 5a by indicating the positions of the solute atoms in the A, B, and C layers. The hexagonal unit cell of $D0_{24}$ structure may be considered as four h c p unit cells stacked on four others such that the lattice parameters of $D0_{24}$ are twice the corresponding lattice parameters of h c p cells. Thus the close-packed (0 0 1) plane of $D0_{24}$ is similar to the (1 1 1) plane of f c c

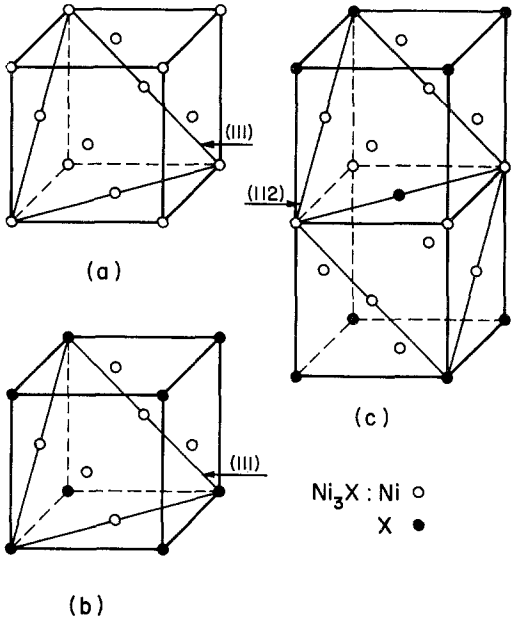

Figure 4 Units cells of (a) Al (f c c), (b) $L1_2$ (γ') and (c) $D0_{22}$ (γ'') structures.

nickel. The atomic arrangement on the (0 0 1) plane of the $D0_{24}$ is shown in Fig. 5b. The ordering of atoms is triangular which is similar to that found in the (1 1 1) plane of the $L1_2$ structure. However, the stacking sequence of the $D0_{24}$ structure, ABAC, is different (Fig. 5b). The hexagonal unit cell of $D0_{19}$ structure consists of four h c p unit cells placed next to each other such that the lattice parameter a of $D0_{19}$ is twice that of h c p structure. The planes of atoms parallel to (0 0 1) are similar to the (1 1 1) planes of f c c and have a perfect close-packed arrangement in Ni_3Sn and a slightly distorted one in Ni_3In. The ordering of solutes in these planes is again triangular, but the stacking sequences is AB (Fig. 5c).

The $D0_{22}$ unit cell is shown in Fig. 4c. It consists of two f c c unit cells stacked one above the other. The (1 1 2) plane of $D0_{22}$ has the same arrangement of atoms at the (1 1 1) plane of nickel (Fig. 5d). Ordering of solute atoms on the (1 1 2) plane (Fig. 5d) is such that alternate rows of atoms containing solute atoms at alternate sites are displaced relative to each other by one interatomic distance along the $[\bar{1}\,1\,0]$ direction. The resulting ordering is rectangular. In order to avoid solute–solute contact the stacking in this structure becomes ABCDEF as indicated in Fig. 5d. The orthorhombic unit cell of Cu_3Ti type structure may be considered as an orthohexagonal unit cell as outlined in the h c p structure in Fig. 6. The b-axis of the orthorhombic unit cell is perpendicular to the plane of the paper in Fig. 6 and is parallel to the c-axis of the h c p structure. In an ideal close-packed arrangement the lattice parameters a, b and c of the orthorhombic cell are in the ratio $2 : (8/3)^{1/2} : 3^{1/2}$. The lattice parameters of Ni_3Nb, Ni_3Ta and Ni_3Mo differ only marginally from the ideal ratios as a contraction of only about 0.7% along the [0 0 1] direction and an expansion of only about 1.8% along the [1 0 0] direction would make the ratios ideal. If the slight distortion is ignored the atomic arrangement in the (0 1 0) plane of the Cu_3Ti structures becomes same as that in the (1 1 1) plane of nickel. Fig. 5e shows that ordering of atoms in this structure is rectangular like that in $D0_{22}$. The stacking sequence, AB, however, is different.

The arrangement of atoms in the (1 1 1), (0 0 1), (1 1 2) and (0 1 0) planes of $L1_2$, $D0_{24}$, $D0_{19}$, $D0_{22}$, and Cu_3Ti type structures is the same as that in the (1 1 1) plane of nickel (Fig. 5f). Similarly (0 0 1) planes of nickel are similar to the (0 0 1) planes of $L1_2$ and (1 0 0) and (0 0 1) planes of $D0_{22}$ (Fig. 4). The ordering is, however, triangular in the $L1_2$, $D0_{24}$, and $D0_{19}$ structures and rectangular in the $D0_{22}$ and Cu_3Ti type structures. The close similarity between the atomic arrangements in various planes is likely to give rise to the formation of coherent interfaces between the nickel-rich matrix and the precipitating compounds.

3.3. Coherency between precipitate and matrix

Coherent interfaces between precipitates and matrix may lead to appreciable strengthening. Relatively small coherency strains and low surface energies associated with coherent precipitates result in uniform distribution of precipitates and high resistance to coarsening. Formation of coherent precipitates is encouraged by a small mismatch. The mismatch, δ, between two planes may be defined as $|(D_p - D_M)/D_M|$ where D represents the interatomic distance along the matching direction in the matching planes at the precipitate–matrix interface. The planes of the f c c matrix and the precipitating compounds which have similar atomic arrangements may form coherent interfaces. The D spacings along ⟨1 1 0⟩ directions on the {1 1 1} planes of nickel [21], ⟨1 1 0⟩ directions on the {1 1 1} planes of $L1_2$, [1 0 0] and [0 1 0] directions on the (0 0 1) planes of $D0_{24}$ and $D0_{19}$, [1 1 0] and [2 0 1] directions on the (1 1 2) plane

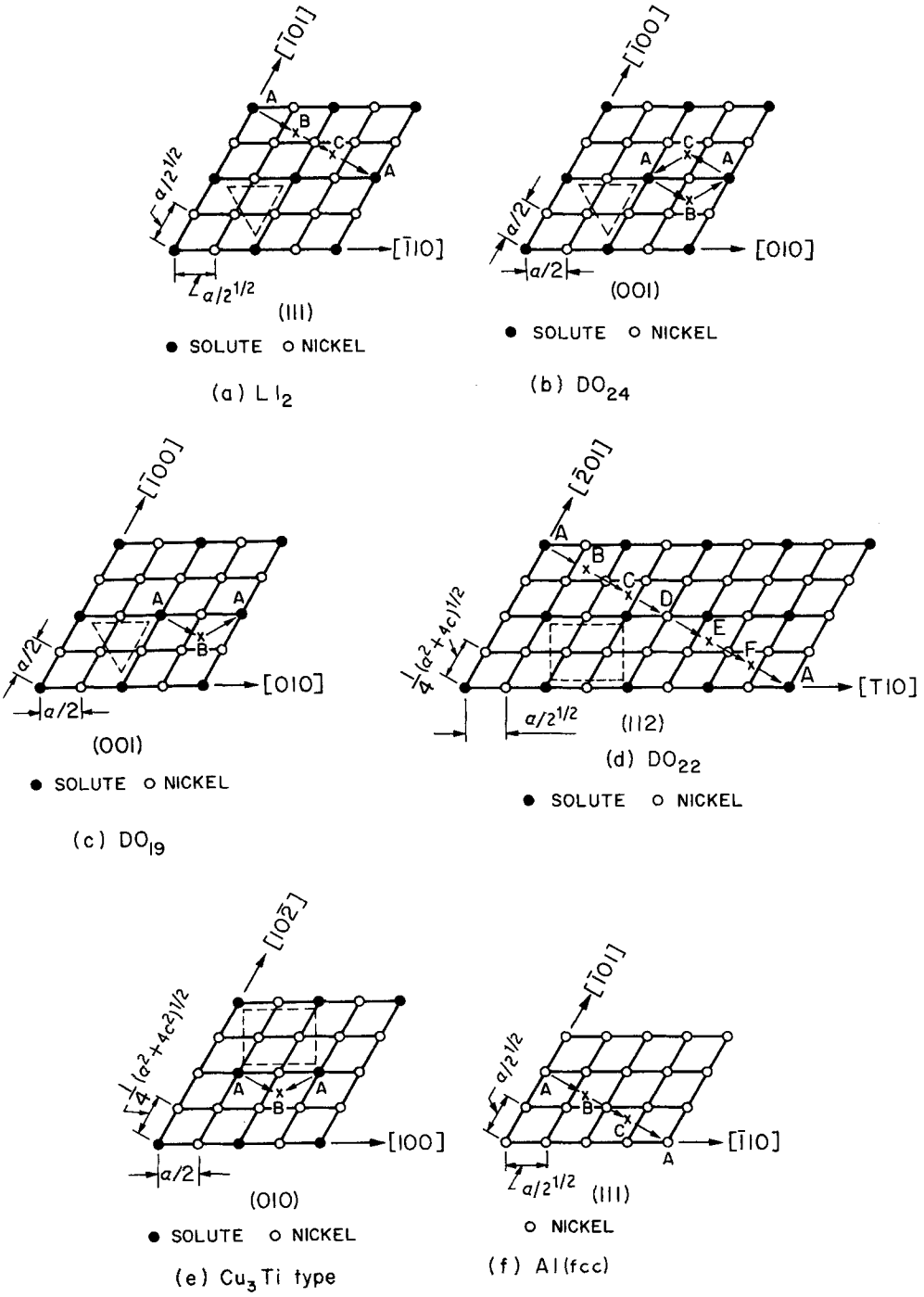

Figure 5 Ordering and stacking sequence in Ni_3X type compounds and nickel.

of DO_{22} and [1 0 0] and [1 0 2] directions on the (0 1 0) plane of Cu_3Ti type structures have been used to calculate mismatch. These values are listed in Table II. The mismatches between the (0 0 1) planes of nickel, $L1_2$ and DO_{22} structures are the same as those listed in this table. The magnitudes of δ are rather high for the formation of coherent precipitates of most of the compounds since the interatomic spacing in nickel is too low. The solid solution forming elements with the exception of only silicon, beryllium and germanium are capable of increasing the lattice parameter of the nickel-rich matrix (Table II) and reducing the mismatch considerably. The most effective elements are

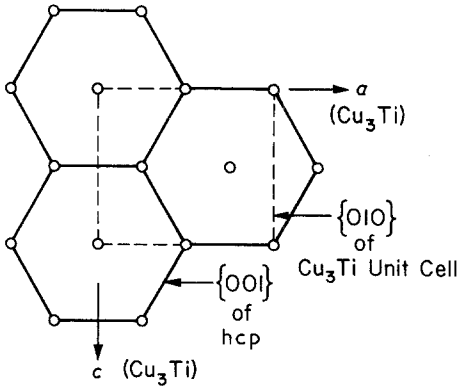

Figure 6 Orthorhombic unit cell of Cu_3Ti type structure outlined as an orthohexagonal unit cell in h c p structure. The *b*-axis of Cu_3Ti is parallel to the *c*-axis of h c p which is perpendicular to the plane of the paper.

niobium, tantalum, tungsten, molybdenum and titanium. Other solutes such as cobalt, iron and chromium become effective when they are present in large quantities. Mismatch increases with time due to a reduction in alloy content of the matrix because of precipitation and differential thermal expansion. Chemical analysis of the matrix of a number of superalloys [24] suggests that cobalt, iron, chromium and molybdenum remain in the martrix during precipitation. These elements have the advantage of maintaining low mismatch during precipitation.

The γ' precipitates of Ni_3Al form coherently on $\{1\,0\,0\}$ planes of the matrix [25] in a nickel-rich alloy containing 18.7% Cr and 5.4% Al. The mismatch in this alloy is only 0.05%. The mismatch is a little higher (0.37 to 0.5%) in Ni–Al alloys but the precipitates are still coherent [26, 27]. The orientation relationship [28] is $\{1\,0\,0\}_M \| \{1\,0\,0\}_{\gamma'}$ and $\langle 1\,0\,0\rangle_M \| \langle 0\,0\,1\rangle_{\gamma'}$. In an Ni–12 at% Ti alloy the hexagonal Ni_3Ti phase, η, precipitates as thin, needle-like Widmanstattten plates [29–31] with $(0\,0\,1)_\eta \| \{1\,1\,1\}_M$, $\langle 1\,1\,\bar{2}\,0\rangle_\eta \| \langle 1\,1\,0\rangle_M$. The Ni–19 at% V alloy gives rise to coherent, disc-like precipitates of γ'' on $\{1\,0\,0\}$ planes of the matrix [32, 33]. The misfit is about 0.3%. The orientation relationship [28] is $\{1\,0\,0\}_M \| [0\,0\,1]_{\gamma''}$. Orthorhombic Ni_3Nb, β, precipitates from a number of niobium-bearing alloys with a considerably reduced mismatch [34–36] of about 0.6 to 1.3% and an orientation relationship [34, 36] given by $(0\,1\,0)_\beta \| \{1\,1\,1\}_M$ and $[1\,0\,0]_\beta \| \langle 1\,1\,0\rangle_M$. Ni–Si alloys also give rise to coherent-precipitates of cubic Ni_3Si with a mismatch of about 0.3% [25, 37]. In all these systems the observed orientation relations are exactly the same as those expected from crystallographic considerations. γ'' precipitates prefer $\{0\,0\,1\}$ planes of the matrix [38] so that their $[0\,0\,1]$ directions may remain parallel to the direction of minimum elastic modulus of the matrix.

The shapes of precipitates are related to strain energy. The magnitude of strain energy is determined by mismatch, orientation and size of the precipitates. Spherical precipitates of γ' form when the mismatch is less than 0.4% [25, 37, 39]. γ' is cubical [25, 37, 39] with $1\% > \delta > 0.4\%$. The cubical shape may be considered as spherical with slight perturbation due to elastic anisotropy. Cellular precipitation of γ' can occur [39] if the mismatch exceeds 1%. When the mismatch exceeds 3% plates or rods of γ' may precipitate [25]. For a given mismatch, strain energy increases with size of the precipitate. The precipitates are, therefore, spherical in the initial stages and change into cubical or plate-like shapes in the later stages of precipitation [27]. The γ'' precipitates are coherent disc-shaped particles [36, 38, 40, 41] or square platelets [34]. The thin long laths of β and η do not appear to change shape with change in mismatch [28, 29, 34–36]. The Ni–Sn alloys containing up to 10 at% Sn have cellular precipitates of Ni_3Sn [42]. The mismatch in these alloys is greater than 3.7%. Morphologies of precipitates with large misfits may change significantly due to annealing under stress; the magnitude of change depends on the direction and sense of the applied stress. Compressive stress anneal develops rods parallel to the stress axis while tensile stress anneal develops platelets perpendicular to the applied stress [43–45].

3.4. Formation of precipitates of metastable phases

The precipitation of equilibrium phases can increase the strength by several hundred per cent [35, 46, 47]. However, certain shapes of precipitates such as the laths of β and η, or cellular precipitates, are not desirable as they reduce ductility and toughness. Only a controlled amount of η and β at the grain boundaries can improve stress rupture resistance [48]. High silicon content tends to promote formation of β, while high aluminimum and tantalum contents retard nucleation of β [49]. Phases with a more suitable shape, size and coherency can become more useful as strengtheners. Ideally small, coherent and uniformly distri-

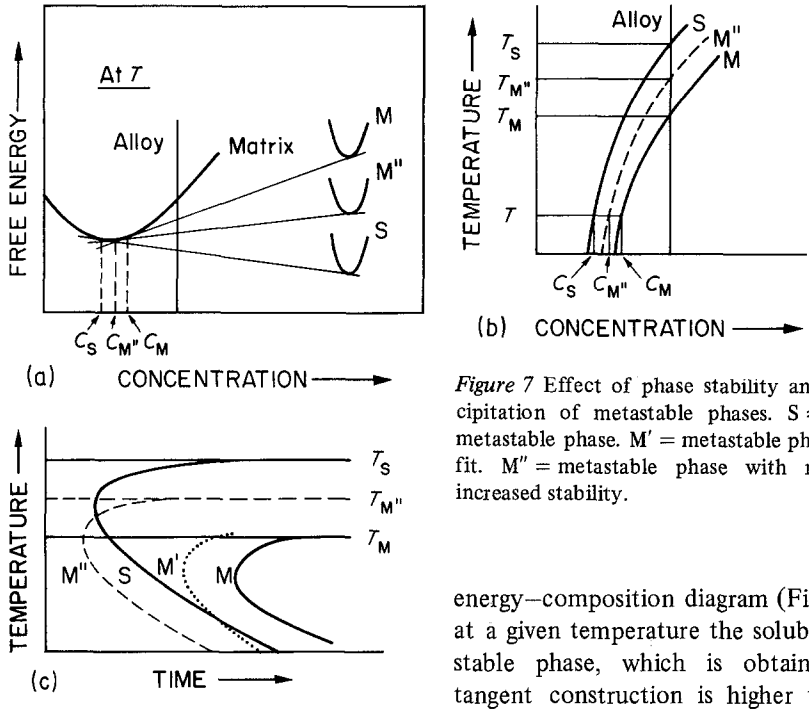

Figure 7 Effect of phase stability and misfit on the precipitation of metastable phases. S = stable phase. M = metastable phase. M′ = metastable phase with reduce misfit. M″ = metastable phase with reduced misfit and increased stability.

buted precipates are required. The γ' ($L1_2$) and γ'' ($D0_{22}$) precipitates meet these requirements. Inducing precipitation of metastable γ' and γ'' in systems in which these phases are not stable is desirable.

Precipitates of metastable γ' and γ'' may be expected to appear when the misfit is small. Some of the niobium-bearing alloys give metastable γ' and γ'' precipitates with misfit less than 1% for γ'' [28, 34, 35] and 1.3% for γ' [28, 40, 41, 50]. Nickel containing 12.5% Ti gives rise to γ' precipitates in the early stages of precipitation with a mismatch of only about 0.6% [51]. A number of other alloys behave in this manner [29, 30, 46, 52]. Molybdenum encourages formation of γ' and suppresses precipitation of η by lowering the mismatch [53]. However, a number of alloys with the mismatch reduced to very low values do not give rise to the precipitation of metastable γ' or γ'' [28, 35]. Such behaviour is attributable to the change in the stability of the precipitates.

Formation of a metastable phase is determined by both its low mismatch and high stability. The role of these two factors in the precipitation of a phase is schematically illustrated in Fig. 7 through free energy–composition, temperature–composition and temperature–time–transformation diagrams of two competing phases; stable phase, S, and metastable phase, M. The free energy–composition diagram (Fig. 7a) shows that at a given temperature the solubility of the metastable phase, which is obtained by common tangent construction is higher than that of the stable phase. Therefore, the solvus of the metastable phase in Fig. 7b is to the right of that of the stable phase and for a given alloy composition the equilibrium solution temperature (T_S) of the stable phase is greater than that (T_M) of the metastable phase. Fig. 7c shows the time required for the initiation of precipitation of the two phases. Since the time required for the initiation of precipitation of the metastable phase is much longer than that of the stable phase, the metastable phase is suppressed. When the misfit of the metastable phase is reduced, its surface energy is considerably decreased and the rate of precipitation of this metastable phase, M′, with reduced misfit is appreciably increased as shown by the dotted curve in Fig. 7c. The equilibrium solution temperature, $T_{M'}$, of the phase M′ may also be increased a little because of decreased strain energy. If, however, substitution results in a considerably reduced misfit as well as increased stability, the metastable phase with low misfit and high stability, M″, may have a free energy composition curve and a solvus line as shown by the dashed line in Figs. 7a and b. The correponding curve for initiation of precipitation is shown in Fig. 7c. It is clear that precipitation of the metastable phase with reduced misfit and increased stability (M″) would be dominant. Substitution of alloying elements in Ni_3X may result in appreciable increase in the stability and decrease of the mismatch of Ni_3X.

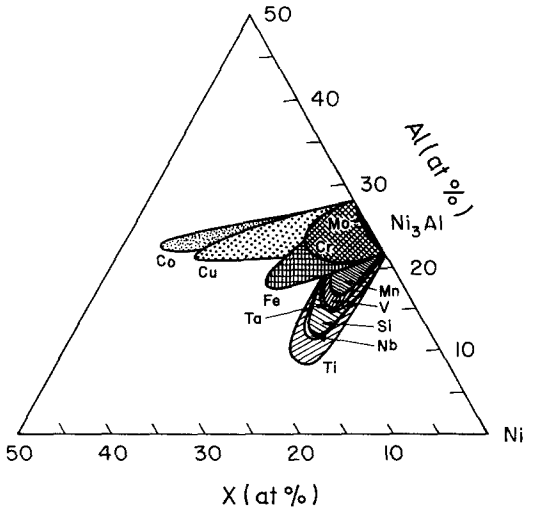

Figure 8 Semischematic solid solution fields of Ni_3Al in a number of Ni–Al–X type ternary systems at about 1400 K [5, 60, 61].

3.4.1. Effect of alloy substitution on mismatch

The alloying elements substitute for both nickel and X in Ni_3X. On the basis of chemical analysis of the matrix and extracted γ' precipitates it has been suggested that cobalt and iron substitute for nickel; chromium substitutes for nickel and aluminium; titanium, niobium, vanadium, tantalum, tungsten and molybdenum substitute for aluminium [24]. However, most of the iron, chromium, cobalt and molybdenum remains in the matrix [24]. Superimposed semi-schematic isothermal sections of Ni_3X fields of ternary systems Ni–Al–X (X = Cu, Co, Fe, Cr, Ti, Nb, V, Mo, Si, Mn, Ta) at about 1400 K are shown in Fig. 8 [5, 54, 55]. It follows from this figure that titanium, niobium, tantalum, vanadium, manganese and silicon substitute for aluminium. Iron, chromium and molybdenum substitute for both aluminium and nickel; cobalt and copper substitute for nickel. On the other hand, very little molybdenum goes into solution into Ni_3Al and η and β take very little aluminium into solution [55–57]. In general, all the Ni_3X forming solute elements may be expected to substitute for X, the extent of substitution being dependent on the relative atomic diameters and the crystal structures of Ni_3X.

Substitution of nickel in Ni_3X by cobalt, iron, chromium, molybdenum and tungsten results in an increase in the lattice parameter of Ni_3X cancelling partly their effect in reducing the mismatch by increasing the lattice parameter of the matrix (Table I). Since these elements are mostly present in the matrix their effect in reducing the mismatch by increasing the lattice parameter of the matrix would predominate. Chromium, iron, molybdenum and tungsten substitute for X in Ni_3X to a minor extent. Therefore, their effect on the mismatch due to change in the lattice parameter of Ni_3X would not be appreciable. Change in the lattice parameter of Ni_3X due to substitution of X by aluminium, titanium, vanadium, tantalum, niobium, gallium, indium, germanium, silicon and tin would depend upon their relative atomic diameters. The percentage difference between atomic diameters of X and the element substituting for X in Ni_3X is obtainable from Table I.

Substitution of aluminium in Ni_3Al by titanium or niobium leads to an increase in the lattice parameter of γ' [57–59]. Substitution of vanadium and silicon for aluminium leads to a decrease in the lattice parameter of Ni_3Al [54]. The elements decreasing the lattice parameter of Ni_3X would generally reduce the mismatch. For example, substitution of niobium in Ni_3Nb by aluminium, vanadium, gallium, silicon and germanium should lead to a decrease in the lattice parameter of Ni_3Nb and a reduction in misfit.

3.4.2. Effect of alloy substitution on stability of phases

Substitution of alloying elements leads to a change in the stability of alloy phases. When niobium is substituted for aluminium in Ni_3Al the degree of long-range order increases by 25% [59]. The changes in relative stabilities of phases may be evaluated in terms of models based on free electron concentration or (s + p) electron concentrations as proposed by Brewer.

3.4.2.1. Approach based on free electron concentration. A survey of A_3B type compounds has shown that the atomic size effect is not very important in determining the stability of these compounds, But the ratio of average total electrons outside the inert gas shell to the number of atoms is the controlling factor [60]. The A_3B type compounds with $L1_2$ structure (γ') are found at electron to atom ratios (e/a) less than 8.65, whereas the compound with $D0_{22}$ structure (γ'') is found at $(e/a) > 8.65$.

The electron concentration in Ni_3X type compounds and their components are listed in Table

TABLE III Ratios of average total electrons outside the inert gas shell to the number of atoms, (e/a), in Ni_3X type compounds

Component	(e/a) in component	Structure of the Ni_3X type compound	Average (e/a) in the compound
Al	3	$L1_2$	8.25
Ti	4	$D0_{24}$	8.5
V	5	$D0_{22}$	8.75
Nb	5	Cu_3Ti type	8.75
Ta	5	Cu_3Ti type	8.75
Mo	6	Cu_3Ti type	9.0
Ga	3	$L1_2$	8.25
In	3	$D0_{19}$	8.25
Si	4	$L1_2$	8.5
Ge	4	$L1_2$	8.5
Sn	4	$D0_{19}$	8.5
Cr	6	—	—
W	6	—	—
Fe	8	—	—
Co	9	—	—
Ni	10	—	—

III. This information can be used for predicting relative stabilities of precipitates. In the Ni–Nb system precipitates of only β are found [28]. However, the Cu–Ni–Nb system yields precipitates of β and γ'' [34]. Partial substitution of nickel by copper in Ni_3Nb reduces its (e/a) ratio, stabilizes γ'' and induces its precipitation. In the presence of aluminium in the Cu–Ni–Nb alloy, aluminium substitutes for niobium in Ni_3Nb and reduces its (e/a) ratio as the corresponding ratio in aluminium is only 3 compared with 5 in niobium (Table III). When the percentage of aluminium is low, γ'' is stabilized. With increase in the percentage of aluminium the (e/a) ratio is further reduced and γ' is stabilized. When the amount of aluminium in the Cu–Ni–Nb system is small, β, γ'' and γ' precipitate at high, intermediate and low ageing temperatures, respectively [40, 41]. Increase in the aluminium content causes precipitation of β and γ' at high and low ageing temperatures and precipitation of γ'' is suppressed. These experimental observations are in accord with the theoretical predictions. Precipitation of γ'' in Ni–Fe–Co–Ta alloys [52] and γ' in Ni–Cr–Fe–Nb–Ti and Ni–Co–Cr–Nb–Al alloys [38, 52] may be interpreted in a similar manner.

This approach can, in principle, be extended to other systems. However, predictions are not always consistent with the experimental observations. Addition of 3% Fe to Ni–12.5% Nb alloy induces precipitation [28] of γ''. This behaviour cannot be attributed to mismatch as it is already very low in the Ni–12.5% Nb alloy. Iron substitutes for both nickel and niobium in Ni_3Nb. Substitution of niobium by iron would only increase the (e/a) ratio and would not stabilize γ''. However, substitution of nickel and iron would decrease the electron concentration and stabilize γ''. Since the electron concentration in chromium is lower than that in iron, chromium would be more effective as a γ'' stabilizer. However, addition of 17% Cr to Ni–Co–Nb alloys [35] does not induce precipitation of γ''. According to Table III addition of vanadium to Ni–Nb alloys should not have any effect. But γ'' is known to precipitate from Ni–Nb–V alloys [33]. Thus the above procedure, which is based on assigning characteristic free electron concentrations to each phase, fails to predict the change in stability of phases in some alloys.

3.4.2.2. Engel–Brewer approach. According to the principles advanced by Brewer [61] each crystal structure is characterized by a definite (s + p) electron to atom ratio. B c c, h c p, $D0_{22}$, $L1_2$, and f c c structures have characteristic ranges of (s + p) electron to atom ratio of 1 to 1.5, 1.75 to 2.25, 2.5 to 2.62, 2.75 to 3.00 and 3.00 respectively [28, 60, 61]. The energy of a crystal structure is determined by the promotion energies of electrons to the appropriate (s + p) configuration and the bonding energies of all the (s + p) and unpaired d electrons. The structure with minimum energy represents the stable phase.

The change in the stabilities of crystal structures with increase in the (s + p) electron concentration is illustrated in Fig. 9. It was shown in Section 3.2 that Cu_3Ti type structure of Ni_3Nb, Ni_3Ta and Ni_3Mo is really a slightly distorted h c p structure with rectangular ordering. Therefore, it would be reasonable to assume that the electron concentration in β is close to those of h c p and $D0_{22}$. The electron concentration in $D0_{24}$ and $D0_{19}$ structures which have triangular ordering are likely to be close to that of the $L1_2$ structure. The probable positions of β, $D0_{24}$ and $D0_{19}$ in the electron concentration scale in Fig. 9 have been indicated.

Iron in the Ni–12.5% Nb alloy behaves as f c c iron since it is part of an f c c lattice. Substitution of nickel by iron in Ni_3Nb should not change the

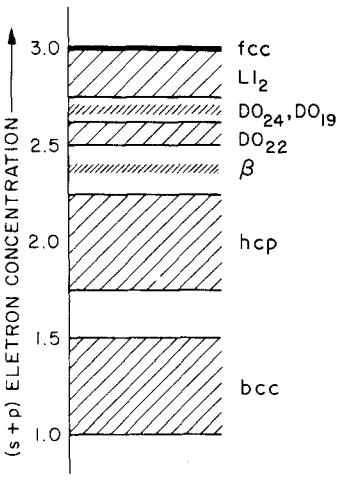

Figure 9 Characteristic (s + p) electron concentrations for the stability of a number of structures.

precipitate stability. But substitution of f c c iron with (s + p) electron concentration of 3 for b c c niobium having (s + p) electron concentration of about 1 results in increase in the (s + p) electron concentration in Ni_3Nb. Therefore, the stability of γ'' relative to β would be increased. Addition of iron does induce precipitation of γ'' [28, 36, 38]. Chromium being b c c, would not encourage precipitation of γ'' [41]. Presence of f c c aluminium stabilizes both γ'' and γ' [28, 40, 50]. Similarly γ'' and γ' in Fe–Ni–Ta [52] and Ni–Cr–Fe–Nb–Ti [38] alloys are stabilized. (s + p) electron concentration in vanadium is about 1.5 compared with one in niobium. Vanadium, therefore, induces precipitation of γ'' in niobium-bearing alloys [47].

Brewer's approach predicts the stability of Ni_3X type compounds more effectively. However, the free electron concentration model is simple and easier to apply.

3.5. Stability of microstructure

The microstructure of a precipitation hardened system consists of precipitates of different sizes distributed in the matrix. The larger precipitates in these systems grow at the expense of smaller ones. It can be shown that when this occurs by volume diffusion-controlled coarsening process the average particle size, $\bar{r}$, is related to the time, t, by the following relation [62]:

$$\bar{r}^3 = \left(\frac{8V^2}{9RT}\right)(\sigma C_e D)t$$

Here V is the molar volume of the precipitate, σ is the energy per unit area of the interface between matrix and precipitate, C_e is the solubility in the matrix and D is the volume diffusion coefficient. The results of a number of investigations suggest that the above volume diffusion-controlled coarsening equation is applicable to the coarsening of γ' and γ'' precipitates in an f c c matrix [26, 27, 32, 36, 46, 50, 63].

It follows from this equation that the coarsening rate may be decreased by reducing interfacial energy, solubility and diffusion coefficients. Reduced misfit increases coherency of the matrix–precipitate interface and reduces the interfacial energy. Solubility is also lowered by the decrease in strain energy due to lowering of misfit. Further reduction in solubility is obtainable through increase in stability of the precipitate. Suitable alloying elements can be substituted in order to improve stability of precipitates. The diffusion coefficients of a number of solutes in nickel at 1000 K which have been plotted in Fig. 2 against the melting temperature of the solutes show that high melting elements have low diffusion coefficients. Thus minimum mismatch and use of high melting solutes for maximization of stability of the precipitates should result in minimum rate of coarsening.

The coarsening rate is reduced by the substitution of aluminium by high-melting titanium in Ni_3Al [58]. Chromium and cobalt can reduce the coarsening rate by decreasing solubility and misfit. Similarly molybdenum and tungsten can reduce the coarsening rate by decreasing misfit and diffusion coefficient. Niobium reduces solubility and the diffusion coefficient [64] and, therefore, lowers the rate of coarsening. Increased coherency strains due to increased misfit may also increase coarsening rate [65]. However, coarsening kinetics do not appear to be significantly influenced by volume fraction of precipitates [66].

Instability in microstructure may also be caused by the destabilization of the f c c matrix of nickel-base superalloys due to the presence of an excess of b c c stabilizing solutes such as chromium, iron, molybdenum, tantalum, niobium and tungsten. The chromium content of superalloys is therefore limited to 15 to 30%. Destabilization of γ may result in the formation of intermetallic compounds like the topographically close packed phases (t c p). These phases precipitate as platelets along grain boundaries. They reduce ductility, decrease stress rupture life and induce brittleness [67, 68]. They

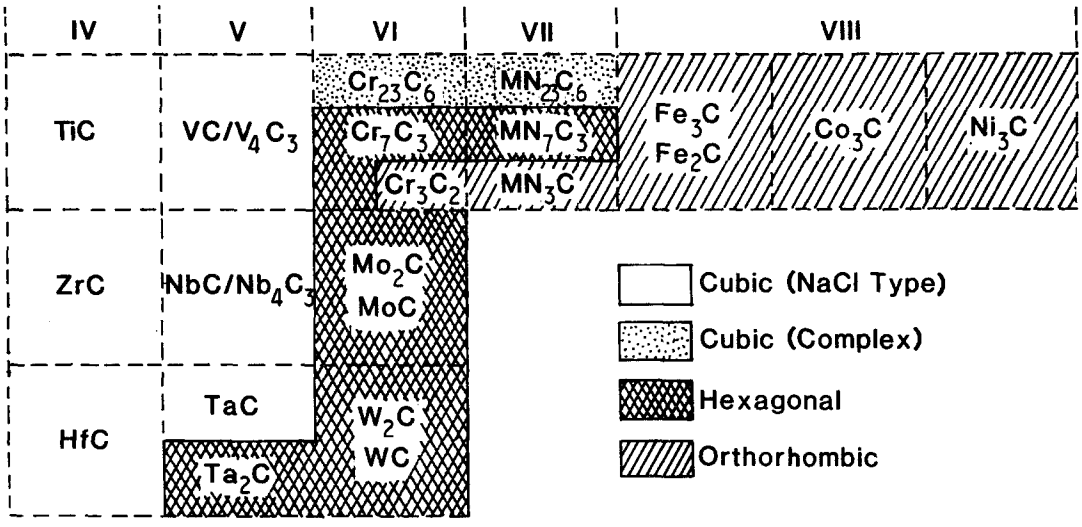

Figure 10 Relationship between structures of carbides and the positions of metals in the Periodic Table (after Goldschmidt [103]).

are the source of crack initiation and propagation in brittle failure. High temperature rupture also occurs along tcp plates [5, 67]. Factors influencing the formation of these phases have been discussed extensively in the literature [69]. Considering electron concentration as the prime factor in determining the stability of tcp phases a computational method, PHACOMP has been developed to predict tcp-free alloy compositions. In this method the average electron vacancy number, $\bar{N}_v$, of the alloy is calculated by the relation

$$\bar{N}_v = \sum_i x_i N_{v,i}$$

where X_i is the atomic fraction of the solute, i, in solid solution in the matrix and N_v is the electron vacancy number of the solute element. A critical value of average electron vacancy number, $\bar{N}_v^*$, below which tcp phases do not form is established. In order to predict the absence of tcp phases the calculated value of $\bar{N}_v$ of an alloy is compared with N_v^*. Several methods based on this principle have been extensively used [70, 71]. A decrease in chromium content generally suppresses the formation of sigma and Laves phases. Iron promotes formation of σ, μ, x, η, and β phases and aluminium, titanium, niobium and silicon promote Laves phases [72].

4. Carbide formers

Carbide-containing nickel-base superallloys have superior creep properties compared with those strengthened by intermetallic compounds. The presence of a network of uniformly distributed discrete carbide particles along the grain boundaries of a superalloy is desirable as it prevents grain-boundary sliding and migration [73]. The optimum effect on properties, however, depends upon the structure and morphologies of carbides. The structure and morphology of carbides are influenced by the alloying elements present in a superalloy. In this section influence of various alloying elements on carbide formation in superalloys is discussed.

The structures of various transition metal carbides are listed in Fig. 10. The cubic MC carbides are most stable and the orthorhombic ones are least stable. Titanium, tantalum, niobium and vanadium stabilize MC type carbides. Other elements destabilize them. Carbides of metals belonging to the same class show considerable intersolubility [8]. The hexagonal carbides of chromium, molybdenum and tungsten are soluble to some extent in cubic carbides, but the orthorhombic carbides show no solubility in cubic ones because of large differences in the atomic sizes of metal atoms. Orthorhombic carbides show some solubility in hexagonal and complex cubic carbides ($M_{23}C_6$). Increasing addition of strong carbide formers results in the formation of carbides in the following general order:

$$M_7C_3 \rightarrow M_{23}C_6 \rightarrow M_6C \rightarrow MC$$

The carbide M_6C in this sequence has a structure

similar to that of $M_{23}C_6$. It is fcc with a lattice parameter of about 1.1 nm.

The presence of strong carbide forming elements results in the formation of MC carbides during solidification. In some alloys a little MC carbide may also precipitate in the solid state where M in MC is titanium, tantalum, niobium, vanadium, molybdenum, tungsten or chromium. None of the orthorhombic carbide forming elements is a part of M. Although hafnium is insoluble in nickel, MC carbides rich in hafnium have been reported in hafnium-containing alloys [80]. The MC carbides are generally angular, cubic- or diamond-shaped blocky particles present at grain boundaries and in the matrix. They have a Chinese script-morphology in some cast alloys [4].

Moderate and high chromium contents ($\gtrsim$ 18%) [75] lead to the formation of $M_{23}C_6$ carbides during solidification, ageing at low temperature or in use. The following reaction leads to the formation of $M_{23}C_6$ carbides at the grain boundaries during ageing:

$$MC + \gamma \rightarrow M_{23}C_6 + \gamma'$$

MC carbide stabilizing elements can retard decomposition of MC. 0.4% niobium decreases the percentage of $M_{23}C_6$ carbides appreciably in Waspaloy [76]. Both cubic and orthorhombic carbide forming elements may become part of M in $M_{23}C_6$ which may be written as (Ni, Co, Fe, Cr)$_{21}$(MoW)$_2$C$_6$. $M_{23}C_6$ carbides at the grain boundaries enveloped within layers of γ' is the ideal morphology for inhibiting grain-boundary sliding and improving creep resistance [5]. The presence of $M_{23}C_6$ carbides as films, plates or discontinuous irregular particles at the grain boundaries results in poor ductility and an increased cracking tendency. Grain-boundary carbides associated with precipitate-free zones due to increased solubility of precipitates as a result of chromium depletion, are also not desirable. Cellular morphology or eutectic colonies reduce ductility, strength and notch rupture strength. Boron is effective in retarding nucleation of cells [5].

The presence of refractory metals such as molybdenum and tungsten over about 8 at% leads to the formation of M_6C type carbides by the reaction [73]:

$$MC + \gamma \rightarrow M_6C + \gamma'$$

Since both orthorhombic and cubic carbide forming elements could be part of M_6C it may be written [6] as (Ni, Co, Cr)$_4$(Mo, W)$_2$C. The M_6C carbides may appear as blocky particles or take the Widmanstatten morphology [4]. The latter is not desirable as it degrades mechanical properties. A high solubility of silicon in M_6C encourages the formation of this carbide [72, 77]. Silicon in the Ni–15Cr–6W–3Mo–2Al–2Ti alloy containing less than 0.4% Si is uniformly distributed. The main carbide in this alloy is $M_{23}C_6$. When the silicon content in the alloy is greater than 0.4%, silicon segregates to the grain boundaries and gives rise to a continuous grain-boundary film of M_6C [77].

The simple Ni–Cr–Al–Ti type of alloys contain Cr_7C_3 carbides as blocky intergranular particles which are generally metastable [4]. They transform to $Cr_{23}C_6$. The morphlogies of various types of carbides and the heat treatment required to evolve those in many commercial alloys have been described in the literature [4, 5, 78].

5. Surface stabilizers

The performance of any engineering materials depends upon the stability of its external and internal interfaces. In this section the influence of various alloying element on the stability of both external as well as internal surfaces of nickel-base superalloys will be briefly reviewed.

5.1. External interface

Instability of external surfaces of nickel-base superalloys in chemically reactive environments leads to degradation of material. Degradation of material can be caused by oxidation at high temperatures in oxidizing atmospheres. When surface reaction occurs in the presence of oxygen, sulphur, sodium, vanadium and other contaminants present in the environment, it is termed hot corrosion. The reaction products of hot corrosion consist of compounds such as molten Na_2SO_4 which dissolve the protective oxide layer of the alloy. The eutectic Ni_3S_2–Ni may also be active during hot corrosion. The mechanisms of oxidation [79, 80] and hot corrosion [81, 82] of superalloys have been discussed elsewhere in the literature and therefore, will not be discussed here.

The presence of chromium in the alloys results in the formation of an oxide layer which reduces further oxidation and hot corrosion. For a good protective layer against oxidation about 20% Cr is required [83]. Optimum nickel content for maximum oxidation resistance is 40 to 50%.

Cobalt is not necessary for adequate oxidation resistance [84, 85]. However, cobalt improves hot corrosion resistance as the diffusivity of sulphur in cobalt is nearly one hundredth of that in nickel and the melting temperature (1150 K) of the Co_4S_3–Co eutectic is higher than that (918 K) of the Ni_3S_2–Ni eutectic [86]. Aluminium additions improve oxidation resistance [87] and resistance to oxide spalling [84]. Above 1223 K aluminium is better than chromium, as Cr_2O_3 tends to form gaseous CrO_3 at these temperatures [88]. Alloys with about 15 at% Cr and 10 at% Al form good protective layers [87]. However, Al_2O_3 provides poor hot corrosion resistance. Compared with aluminium, titanium imparts poor oxidation resistance. Titanium also increases the tendency for intergranular oxidation. However, it does improve hot corrosion resistance. The corrosion rate tends to increase linearly [82] with $[Al]/[Ti][Cr]^{1/2}$. The refractory metals molybdenum and tungsten improve resistance to both oxidation and spalling in some alloys [88, 89]. The effect of the presence of molybdenum, tungsten, niobium and tantalum on hot corrosion resistance is dependent on test conditions [82]. Silicon and manganese, when present up to 1 to 3%, improve oxidation resistance [90]. However, silicon in the presence of aluminium, tantalum and yttrium tends to promote oxide spalling [84]. Addition of rare earths increases the adherency of oxide scales with the metal and improve oxidation [80] and hot corrosion [91, 92] resistance. Rare earths also form low melting Ni–Ni_5R eutectics which give low rupture strength. This may be avoided by adding rare earth oxides [91]. Rare earth oxides also improve hot corrosion resistance by reacting with sulphur [92]. Minor additions of reactive elements such as yttrium, lanthanum and caesium improve oxidation resistance [80, 84].

5.2. Internal interfaces

These are primarily grain boundaries. It has been observed that the presence of discrete particles of $M_{23}C_6$ at the grain boundary can stabilize the grain boundaries against grain-boundary sliding and migration during application at elevated temperatures. However, a number of elements have a tendency to segregate to the grain boundary, weaken it and initiate cracks along it. Elements insoluble in nickel such as lead, bismuth, thallium and tellurium present as impurities in trace amounts cause such embrittlement [93, 94]. Phosphorus also causes cracking and hot tearing [21, 95]. Sulphur segregates to the grain boundaries [26, 102] and its concentration at the boundaries can go up to 12 at% in alloys containing only 0.006 at% S [96]. Sulphur causes loss of ductility due to the presence of a low melting eutectic at the grain boundaries.

It was pointed out in Section 3 that some of the solid solution forming elements, arsenic, antimony, copper, manganese and silicon also segregate [18–20] to the grain boundaries and cause grain-boundary cracking [18–21]. Manganese is useful in counteracting sulphur: it gives rise to globular particles of MnS at the grain boundaries. Excess manganese (> 1%) improves oxidation resistance [90] and weldability [8]. However, because of loss of ductility, excess manganese is restricted to 0.2 to 1%. Silicon improves oxidation resistance [90], but, because of its embrittling effect [18] and its influence on promoting M_6C carbides [77] and Laves phases [72] at the grain boundaries, it is restricted to 0.2 to 1%.

A few elements tend to impart beneficial properties to the alloy by segregating to the grain boundaries. These elements stabilize the grain boundary against premature cracking. The effect of small additions of boron (~ 0.009%) is to improve hot ductility and rupture life [97]. Boron segregates to the grain boundaries [98] and prevents rapid agglomeration of $M_{23}C_6$ carbides possibly due to reduced grain-boundary diffusivity [6]. Excess boron forms complex borides with molybdenum, titanium, chromium and nickel. A small percentage of zirconium (~ 0.01%) improves hot ductility and rupture life [97]. Zirconium segregates to the grain boundaries, combines with carbon and sulphur to form carbides and carbosulphides [20, 99] and reduces the detrimental effects of sulphur. Like boron, zirconium reduces the agglomeration rate of $M_{23}C_6$ possibly by reducing grain-boundary diffusivity. Magnesium improves the stress rupture life [100] by reacting with interstitial impurities, oxygen, nitrogen and sulphur and nulifying their harmful effects. Magnesium also gives rise to finely dispersed intragranular particles of sulphide. Hafnium improves rupture life and ductility [101] by acting as a getter [99] to prevent grain-boundary embrittlement caused by sulphur. It enters carbides and γ' particles [74]. Rare earths improve the ductility and stress rupture life by reducing the sulphur

content of the alloy [102]. Most of the beneficial elements improve properties by eliminating sulphur. However, the role of boron is not yet well understood.

6. Conclusions

The constituents of nickel-base superalloys may be classified into matrix formers, solid solution formers, precipitate formers, carbide formers and surface stabilizers. Elements with face centred cubic structures, and having high melting points and significant solubility for a number of elements are suitable as matrix formers. Nickel is one such element. Out of thirty elements which have significant solubility in nickel, the solutes tungsten, molybdenum, titanium, tantalum, niobium, vanadium, rhenium and technetium have favourable characteristics for hardening the nickel-rich matrix by solid solution formation.

The solutes aluminium, titanium, vanadium, niobium, tantalum, molybdenum, gallium, indium, silicon, germanium and tin form Ni_3X type compounds. These compounds have widely different structures, but the atomic arrangements in them turn out to be similar to that in nickel. They may strengthen the matrix by forming coherent precipitates of stable and metastable phases provided the mismatch is low and the stability of the precipitating phase is high. Changes in mismatch and stability are predictable by considering suitable alloy substitution. The relative stabilities of phases can be assessed using the Engel–Brewer theory. The free electron approach to stability is found to be not always applicable. Resistance to precipitate coarsening, formation of tcp phases from the matrix and stabilities of various types of carbides can be controlled by regulating the alloying additions.

Resistance to external surface degradation by oxidation and hot corrosion is controlled primarily by chromium, aluminium, titanium and rare earth additions. Embrittling of internal surfaces like grain boundaries by segregating solutes and impurities can be alleviated by minor additions of boron, zirconium, magnesium, hafnium and rare earths.

This review indicates the areas in which suffient experimental data are not yet available. The effect of grain-boundary segregation and homogenization of solid solution forming elements such as tin and manganese are not yet well established. The solid solution hardening coefficients of a large number of solutes are not known. Data on precipitation in tantalum, molybdenum, gallium, indium, germanium and tin bearing nickel-base systems are scanty. Very little information is available on the extent of substitution of elements such as aluminium, titanium, vanadium, niobium, tantalum, molybdenum, gallium, indium, silicon, germanium and tin for each other in Ni_3X and their effect on lattice mismatch, precipitate stability and coarsening rate. The role of minor additions in improving carbide morphology and surface stability should be further explored.

Acknowledgements

The authors would like to thank the Natural Science and Engineering Research Council of Canada and the University of Manitoba Research Board for the financial support. Thanks are also due to Dr J. R. Cahoon of the University of Manitoba, Mechanical Engineering Department for many useful discussions.

References

1. M. J. WAHLL, D. J. MAYKUTH and H. J. HUCEK, in "Handbook of Superalloys" (Battelle Press, Columbus, 1979) p. 1.
2. R. W. FAWLEY, in "The Superalloys", edited by C. T. Sims and W. C. Hagel (Wiley, New York, 1972) p. 3.
3. P. S. KOTVAL, *Metallogr.* **1** (1969) 251.
4. G. P. SABOL and R. STICKLER, *Phys. Status Solidi* **35** (11) (1969) 11.
5. R. F. DECKER and C. T. SIMS, in "The Superalloys", edited by C. T. Sims and W. C. Hagel (Wiley, New York, 1979) p. 33.
6. R. T. HOLT and W. WALLACE, *Int. Metals Rev.* **21** (1976) 1.
7. OLEG D. SHERBY and PETER M. BURKE, *Progr. Mater. Sci.* **13** (7) (1967) 325.
8. W. HUME-ROTHERY and G. V. RAYNOR, "The Structure of Metals and Alloys", 4th Edn. (Revised) (The Institute of Metals, London, 1967) p. 91.
9. M. HANSEN and K. ANDERKO, "Constitution of Binary Alloys", 2nd Edn. (McGraw Hill, New York, 1958); R. P. Elliott, first supplement (1965); F. A. Shunk, second supplement (1969).
10. R. M. N. PELLOUX and N. J. GRANT, *Trans. Met. Soc. AIME* **218** (1960) 232.
11. B. E. P. BEESTON and L. K. FRANCE, *J. Inst. Metals* **96** (1969) 105.
12. P. C. J. GALLAGHER, *Met. Trans.* **1** (1970) 2429.
13. W. B. PEARSON, "A Handbook of Lattice Spacing and Structures of Metals and Alloys" (Pergamon Press, Oxford, 1967).
14. A. K. JENA, D. GULATI and T. R. RAMACHANDRAN, *Z. Metalkde* **39** (1948) 111.
15. C. J. SMITHELLS, "Metals Reference Book", 5th Edn. (Butterworths, London, 1976) p. 860.

16. W. KOSTER and W. RAUSCHER, *Z. Metalkde* **39** (1948) 111.
17. L. W. WOODYATT, C. T. SIMS and H. J. BEATTIE, *Trans. AIME* **236** (1966) 519.
18. M. SAKAKIBARA and S. SEKINO, in "Superalloy Processing" (Metals and Ceramics Information Centre, Battelle, Columbus, Ohio, 1972) p. I-1.
19. Y. S. WANG, X. M. GUAN, H. Q. YE, J. BI and A. S. XU, in "Superalloys 1980" (ASM, 1980) p. 63.
20. C. L. WHITE, J. H. SCHREIBEL and R. A. PADGETT, *Met. Trans.* **14A** (1983) 595.
21. C. L. WHITE and R. A. PADGETT, *Scripta Metall.* **16** (1982) 461.
22. P. M. KELLY, *Int. Met. Rev.* **18** (1973) 31.
23. P. NASH and D. R. F. WEST, *Met. Sci.* **17** (1983) 99.
24. O. H. KRIEGE and J. M. BARIS, *Trans. ASM* **62** (1969) 195.
25. E. HORNBOGEN and M. ROTH, *Z. Metalkde* **58** (1967) 842.
26. A. J. ARDELL and R. B. NICHOLSON, *J. Phys. Chem. Solids* **27** (1966) 1793.
27. *Idem, Acta Metall.* **14** (1966) 1295.
28. W. E. QUIST, R. TAGGART and D. H. POLONIS, *Met. Trans.* **2** (1971) 825.
29. K. SAITO and R. WATANABE, *Jap. J. Appl. Phys.* **8** (1969) 14.
30. D. H. BEN ISRAEL and M. E. FINE, *Acta Metall.* **11** (1963) 1051.
31. B. R. CLARK and F. B. PICKERING, *J. Iron Steel Inst.* **205** (1967) 70.
32. H. A. MOREEN, R. TAGGART and D. H. POLONIS, *Met. Trans.* **5** (1974) 79.
33. *Idem, Metallogr.* **7** (1974) 513.
34. M. RAGHAVAN, *Met. Trans.* **8A** (1977) 1071.
35. D. W. CHUNG and M. C. CHATURVEDI, *Met. Sci.* **8** (1974) 215.
36. M. C. CHATURVEDI and D. W. CHUNG, *Met. Trans.* **10** (1979) 1579.
37. J. MANENC, *Acta Metall.* **7** (1959) 124.
38. I. KIRMAN and D. H. WARRINGTON, *J. Iron Steel Inst.* **205** (1967) 1264; **99** (1971) 197.
39. W. C. HAGEL and H. J. BEATTIE, in "Precipitation Processes in Steel" (The Iron and Steel Institute, London, 1959) p. 98.
40. M. RAGHAVAN, *Met. Trans.* **9A** (1978) 734.
41. *Idem, ibid.* **10A** (1979) 1399.
42. M. FREBEL, B. PREDEL and U. KLISA, *Z. Metalkde* **65** (1974) 311.
43. J. K. TIEN and R. P. GAMBLE, *Met. Trans.* **3** (1972) 2157.
44. T. MIYAZAKI, K. NAKAMURA and H. MORI, *J. Mater. Sci.* **14** (1979) 1827.
45. D. D. PEARSON, F. D. LEMKEY and B. H. KEAR, in "Superalloys 1980" (ASM, 1980) p. 513.
46. S. E. AXTER and D. H. POLONIS, *Meter. Sci. Eng.* **36** (1978) 71.
47. A. K. JENA and M. C. CHATURVEDI, to be published.
48. J. H. MOLL, G. N. MANIAR and D. R. MUZYKA, *Met. Trans.* **2** (1971) 2153.
49. C. P. SULLIVAN and M. J. DONACHIE, *Met. Eng. Q.* **11**(4) (1971) 1.
50. C. RAVINDRAN and M. C. CHATURVEDI, *Met. Trans.* **6a** (1975) 213.
51. J. R. MIHALISIN and R. F. DECKER, *Trans. AIME* **218** (1960) 507.
52. R. COZAR and A. PINEAU, *Met. Trans.* **5** (1974) 2471.
53. D. RAYNOR and J. M. SILCOCK, *Metal Sci. J.* **4** (1970) 121.
54. R. W. GUARD and J. H. WESTBROOK, *Trans. AIME* **215** (1959) 807.
55. P. NASH and D. R. F. WEST, *Met. Sci.* **13** (1979) 670.
56. A. TAYLOR and R. W. FLOYD, *J. Inst. Metals* **81** (1952–53) 25.
57. E. L. RAYMOND and D. A. WELLS, in "Superalloy Processing" (Metals and Ceramics Information Center, Battelle, Columbus, Ohio 1972) p. N-1.
58. R. NORDHEIM and N. J. GRANT, *Trans. AIME* **200** (1954) 211.
59. E. C. GUO and F. J. MA, in "Superalloys 1980" (ASM, 1980) p. 431.
60. W. HUME-ROTHERY, *Progr. Mater. Sci.* **13**(5) (1967) 229.
61. L. BREWER, UCRL Report 10701 (University of California, Berkeley, 1964); "High Strength Materials", edited by V. F. Zackay (Wiley, New York, 1965) Ch. 2.
62. C. WAGNER, *Z. Electrochem.* **65** (1961) 581.
63. YA-FANG HAN, P. DEB and M. C. CHATURVEDI, *Met. Sci.* **16** (1982) 555.
64. W. I. MITCHELL, *Z. Metalkde* **55** (1964) 613.
65. E. A. FELL, *Metallurgia* **63** (1961) 157.
66. D. W. CHUNG and M. C. CHATURVEDI, *Metallogr.* **8** (1975) 329.
67. G. CHEN, X. XIE, K. NI, Z. XU, D. WANG, M. ZHANG and Y. JU, in "Superalloys 1980" (ASM, 1980) p. 323.
68. G. CHEN, C. YAO, Z. ZHONG and W. YU, in "Superalloys 1980" (ASM, 1980) p. 355.
69. C. T. SIMS, in "The Superalloys", edited by C. T. Sims and W. C. Hagel (Wiley, New York, 1972) p. 259.
70. L. R. WOODYATT, C. T. SIMS and H. J. BEATTIE, *Trans. AIME* **236** (1966) 519.
71. J. R. MIHALISIN, C. G. BIEBER and R. T. GRANT, *Trans. AIME* **242** (1968) 2399.
72. F. J. RIZZO and J. D. BUZZANELL, *J. Metals* **21**(10) (1969) 24.
73. C. T. SIMS, *ibid.* **18** (1966) 1119.
74. C. LUND and J. F. RADAVICH, in "Superalloys 1980" (ASM, 1980) p. 85.
75. H. J. BEATTIE and W. C. HAGEL, *Trans. AIME* **233** (1965) 277.
76. L. A. JACKMAN, H. B. CANADA and F. E. SCZERZENIE, in "Superalloys 1980" (ASM, 1980) p. 365.
77. Y. S. WANG, X. M. GUAN, H. Q. YE, J. BI and A. S. XU, *ibid.*, p. 63.
78. H. E. COLLINS, *Trans. ASM* **62** (1969) 82.
79. G. E. WASIELEWSKI and R. A. RAPP, in "The Superalloys", edited by C. T. Sims and W. C. Hagel

(Wiley, New York, 1972) p. 287.
80. D. P. WHITTLE and J. STRINGER, *Phil. Trans. Roy. Soc. Lond.* **A295** (1980) 309.
81. A. M. BELTRAN and D. A. SHORES, in "The Superalloys", edited by C. T. Sims and W. C. Hagel (Wiley, New York, 1972) p. 317.
82. R. MORBIOLI and H. GILDER, in "High Temperature Alloys for Gas Turbines", edited by D. Coutsouradis, P. Felix, H. Fischmeister, L. Habraken, Y. Lindblom and M. O. Speidel (Applied Science, London, 1978) p. 125.
83. G. S. GIGGINS and F. S. PETTIT, *Trans. Met. Soc. AIME* **245** (1969) 2495.
84. E. P. WHELAN, in "Superalloys 1980" (ASM, 1980) p. 53.
85. A. U. SEYBOLT, G.E. Research Conference Report 70-C-189, June (1970).
86. A. U. SEYBOLT and A. M. BELTRAM, "Hot Corrosion Problems Associated with Gas Turbines", STP421 (American Society for Testing and Materials, 1967).
87. G. R. WALLWORK and A. Z. HED, *Oxidat. Metals* **3** (1971) 171.
88. D. P. WHITTLE, in "High Temperature Alloys for Gas Turbines", edited by D. Coutsouradis, P. Felix, H. Fischmeister, L. Habraken, Y. Lindblom and M. O. Speidel (Applied Science, London, 1978) p. 109.
89. K. R. PETERS, D. P. WHITTLE and J. STRINGER, *Corrosion Sci.* **16** (1976) 791.
90. D. L. DOUGLASS and J. S. ARMIJO, *Oxidat. Metals* **2** (1970) 207.
91. A. U. SEYBOLT, *Corrosion Sci.* **11** (1971) 751.
92. P. ELLIOT and T. K. ROSS, *Werkstoffe u. Korrosion* **72** (1971) 531.
93. G. B. THOMAS and T. B. GIBBONS, in "Superalloys 1980" (ASM, 1980) p. 699.
94. D. R. WOOD and R. M. COOK, *Metallurgia* **67** (1963) 109.
95. D. A. VERMILYEA, C. S. TEDMON and D. E. BROECKER, *Corrosion* **31** (1975) 222.
96. W. C. JOHNSON, J. E. DOHERTY, B. H. KEAR and A. F. GIAMEI, *Scripta Metall.* 8 (1974) 971.
97. R. F. DECKER and J. W. FREEMAN, *Trans. AIME* **218** (1961) 277.
98. J. M. WALSH and B. H. KEAR, *Met. Trans.* **6** (1975) 226.
99. J. E. DOHERTY, A. F. GIAMEI and B. H. KEAR, *Canad. Met. Q.* **13** (1974) 229.
100. R. S. CREMISIO, *Elec. Furn. Steel. Conf. Proc.* **29** (1971) 19.
101. D. N. DUHL and C. P. SULLIVAN, *J. Metals* **23**(7) (1971) 88.
102. T. V. SVISTUNOVA and G. V. ESTULIN, *Stal'* **9** (1963) 725.
103. H. J. GOLDSCHMIDT, *J. Iron Steel Inst. (Lond.)* **160** (1948) 345; quoted in C. S. Barret, "Structure of Metals" (McGraw-Hill, New York, 1952) p. 247.

Received 7 October
and accepted 3 November 1983